

Low specific on-resistance GaN-based vertical heterostructure field effect transistors with nonuniform doping superjunctions

Wei Mao(毛维), Hai-Yong Wang(王海永), Peng-Hao Shi(石朋毫), Xiao-Fei Wang(王晓飞), Ming Du(杜鸣), Xue-Feng Zheng(郑雪峰), Chong Wang(王冲), Xiao-Hua Ma(马晓华), Jin-Cheng Zhang(张进成), Yue Hao(郝跃)
Citation: Chin. Phys. B . 2018, 27(4): 047305. **doi:** 10.1088/1674-1056/27/4/047305

Journal homepage: http://cpb.iphy.ac.cn; http://iopscience.iop.org/cpb

What follows is a list of articles you may be interested in

Analysis of the modulation mechanisms of the electric field and breakdown performance in AlGaN/GaN HEMT with a T-shaped field-plate

Wei Mao(毛维), Ju-Sheng Fan(范举胜), Ming Du(杜鸣), Jin-Feng Zhang(张金风), Xue-Feng Zheng(郑雪峰), Chong Wang(王冲), Xiao-Hua Ma(马晓华), Jin-Cheng Zhang(张进成), Yue Hao(郝跃)
Chin. Phys. B . 2016, 25(12): 127305. **doi:** 10.1088/1674-1056/25/12/127305

Effect of gate length on breakdown voltage in AlGaN/GaN high-electron-mobility transistor

Jun Luo(罗俊), Sheng-Lei Zhao(赵胜雷), Min-Han Mi(宓珉瀚), Wei-Wei Chen(陈伟伟), Bin Hou(侯斌), Jin-Cheng Zhang(张进成), Xiao-Hua Ma(马晓华), Yue Hao(郝跃)
Chin. Phys. B . 2016, 25(2): 027303. **doi:** 10.1088/1674-1056/25/2/027303

A uniform doping ultra-thin SOI LDMOS with accumulation-mode extended gate and back-side etching technology

Yan-Hui Zhang(张彦辉), Jie Wei(魏杰), Chao Yin(尹超), Qiao Tan(谭桥), Jian-Ping Liu(刘建平), Peng-Cheng Li(李鹏程), Xiao-Rong Luo(罗小蓉)
Chin. Phys. B . 2016, 25(2): 027306. **doi:** 10.1088/1674-1056/25/2/027306

Reverse blocking characteristics and mechanisms in Schottky-drainAlGaN/GaN HEMT with a drain field plate and floating field plates

Wei Mao(毛维), Wei-Bo She(佘伟波), Cui Yang(杨翠), Jin-Feng Zhang(张金风), Xue-Feng Zheng(郑雪峰), Chong Wang(王冲), Yue Hao(郝跃)
Chin. Phys. B . 2016, 25(1): 017303. **doi:** 10.1088/1674-1056/25/1/017303

An ultra-low specific on-resistance trench LDMOS with a U-shaped gate and accumulation layer

Li Peng-Cheng, Luo Xiao-Rong, Luo Yin-Chun, Zhou Kun, Shi Xian-Long, Zhang Yan-Hui, Lv Meng-Shan
Chin. Phys. B . 2015, 24(4): 047304. **doi:** 10.1088/1674-1056/24/4/047304

Low specific on-resistance GaN-based vertical heterostructure field effect transistors with nonuniform doping superjunctions*

Wei Mao(毛维)[1], Hai-Yong Wang(王海永)[1], Peng-Hao Shi(石朋毫)[1], Xiao-Fei Wang(王晓飞)[2,†], Ming Du(杜鸣)[1], Xue-Feng Zheng(郑雪峰)[1], Chong Wang(王冲)[1], Xiao-Hua Ma(马晓华)[1], Jin-Cheng Zhang(张进成)[1], and Yue Hao(郝跃)[1]

[1] *Key Laboratory of Ministry of Education for Wide Band-Gap Semiconductor Materials and Devices, School of Microelectronics, Xidian University, Xi'an* 710071, *China*

[2] *School of Microelectronics, Xi'an Jiaotong University, Xi'an* 710049, *China*

(Received 21 December 2017; revised manuscript received 8 February 2018; published online 10 March 2018)

A novel GaN-based vertical heterostructure field effect transistor (HFET) with nonuniform doping superjunctions (non-SJ HFET) is proposed and studied by Silvaco-ATLAS, for minimizing the specific on-resistance ($R_{on}A$) at no expense of breakdown voltage (BV). The feature of non-SJ HFET lies in the nonuniform doping concentration from top to bottom in the n- and p-pillars, which is different from that of the conventional GaN-based vertical HFET with uniform doping superjunctions (un-SJ HFET). A physically intrinsic mechanism for the nonuniform doping superjunction (non-SJ) to further reduce $R_{on}A$ at no expense of BV is investigated and revealed in detail. The design, related to the structure parameters of non-SJ, is optimized to minimize the $R_{on}A$ on the basis of the same BV as that of un-SJ HFET. Optimized simulation results show that the reduction in $R_{on}A$ depends on the doping concentrations and thickness values of the light and heavy doping parts in non-SJ. The maximum reduction of more than 51% in $R_{on}A$ could be achieved with a BV of 1890 V. These results could demonstrate the superiority of non-SJ HFET in minimizing $R_{on}A$ and provide a useful reference for further developing the GaN-based vertical HFETs.

Keywords: GaN-based vertical HFETs, nonuniform doping superjunctions, minimized specific on-resistance, breakdown voltage

PACS: 73.40.Kp, 85.30.Tv, 85.30.De **DOI:** 10.1088/1674-1056/27/4/047305

1. Introduction

The desire for power electronic systems with increasingly excellent performances has been the catalyst for developing GaN-based power devices, in which the vertical GaN-based heterostructure field effect transistor (GaN-based V-HFET), as a kind of high-power switch device, has been attracting increasing attention. Compared with its lateral counterpart (GaN-based HEMT),[1–6] the GaN-based V-HFET has the superiorities, i.e., the reduced chip area, the packaging convenience and the suppression of current collapse,[7] which makes it significantly advantageous and perhaps the only topology choice for power conversions beyond 15 kW.[8] In a high power system, it has been one of the most important focuses to minimize the system power loss. Therefore, the reduction of the specific on-resistance in GaN-based V-HFET is strongly required to reduce the power device loss even at high frequency operation,[9] which depends on a better trade-off characteristic between breakdown voltage (BV) and specific on-resistance ($R_{on}A$).

Recently, a great deal of effort has been made to develop the device structures and fabrication process for GaN-based V-HFETs. Many novel V-HFET structures have been proposed to further improve the trade-off between BV and $R_{on}A$,[10–13] of which the GaN-based V-HFET with uniform doping superjunction (un-SJ HFET) could be considered as the most effective and promising candidate.[11] Furthermore, the successful applications of the etching technology, the regrowth technology and the implantation technology in the fabrication of GaN-based V-HFETs[7,8,14–16] have enhanced the possibility of realizing various novel vertical device structures. These advances are a great encouragement to the further study of GaN-based V-HFETs.

In this paper, a novel GaN-based V-HFET with nonuniform doping superjunction (non-SJ HFET) is presented and investigated. The study of this device emphasizes the further reduction in $R_{on}A$ with the same BV as that of the conventional un-SJ HFET. Compared with un-SJ HFET, the non-SJ HFET has an obvious feature that is the nonuniform doping superjunction (non-SJ) comprising nonuniform doping n- and p-pillars. Based on this, the specific on-resistance could be remarkably reduced without any loss of BV. Two-dimensional numerical simulation with Silvaco-ATLAS software is performed to reveal the intrinsic operation mechanism for the non-SJ by using the potential distributions, electric field dis-

*Project supported by the National Natural Science Foundation of China (Grant Nos. 61574112, 61334002, 61474091, and 61574110) and the Natural Science Basic Research Plan in Shaanxi Province, China (Grant No. 605119425012).

†Corresponding author. E-mail: mxfwang@xjtu.edu.cn

© 2018 Chinese Physical Society and IOP Publishing Ltd

tributions and current density distributions. The relationship among the $R_{on}A$, the BV and the structure parameters of the non-SJ is studied systematically, aiming at optimizing the minimized $R_{on}A$. These results are of importance for designing and further developing the GaN-based V-HFETs.

2. Device structures and physic models

Figure 1 shows the schematic cross-sections of the proposed GaN-based non-SJ HFET and the conventional GaN-based un-SJ HFET. Except for the superjunction, structures for both devices are the same, whose main parameters are given in Table 1. In GaN-based non-SJ HFET, both n- and p-pillars are divided into two parts. The same thickness H_1 and doping concentration N_1 are used in both the top part N_{N1} of the n-pillar and the bottom part P_{P1} of the p-pillar. The same thickness H_2 and doping concentration N_2 are used in both the bottom part N_{N2} of the n-pillar and the top part P_{P2} of the p-pillar. The doping concentration increment, namely N_2 minus N_1, is defined as N_{step}. In addition, the doping concentration of n- and p-pillars in un-SJ HFET is always equal to that of the top part N_{N1} of the n-pillar in non-SJ HFET. For convenience and simplicity, typical N_1 concentrations, namely 0.5×10^{16} cm^{-3}, 1×10^{16} cm^{-3}, 1.5×10^{16} cm^{-3} or 2×10^{16} cm^{-3}, are utilized in simulations, respectively.

Two-dimensional device simulations are performed by using the Silvaco-ATLAS. The polarization effect is considered at each of the P^+-GaN cap/$Al_{0.15}Ga_{0.85}N$ and $Al_{0.15}Ga_{0.85}N$/GaN channel interfaces, according to the experimental reports.[17] Caughey–Thomas mobility model is used based on the experimental measurements.[18] Carrier generation and recombination models, including the impact ionization model,[19] the SRH recombination model and the Auger recombination model are also included in the simulation. Other material physical parameters for GaN and $Al_{0.15}Ga_{0.85}N$ are adopted according to the reports.[20,21]

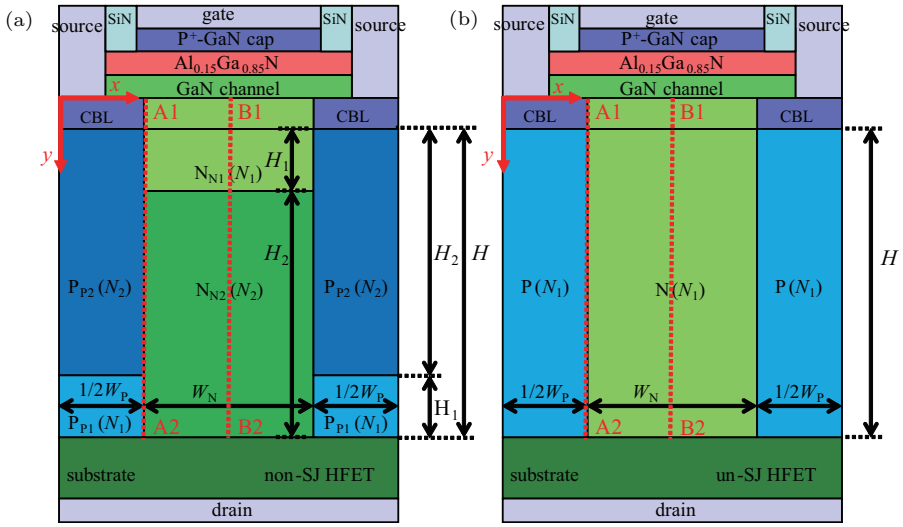


Fig. 1. (color online) Schematic structures for (a) non-SJ HFET and (b) un-SJ HFET. Lines A1A2 or B1B2 denote the vertical direction at the n-pillar/p-pillar junction or the middle of the device, respectively.

Table 1. Main structure specifications for non-SJ HFET and un-SJ HFET.

Symbol	Description	Values
T_{cap}/nm	P^+-GaN cap thickness	100
N_{cap}/cm^{-3}	P^+-GaN cap doping concentration	1×10^{18}
T_{AlGaN}/nm	unintentionally doped $Al_{0.15}Ga_{0.85}N$ thickness	30
$T_{channel}$/nm	GaN channel thickness	120
$N_{channel}$/cm^{-3}	GaN channel doping concentration	2×10^{16}
T_{CBL}/μm	current blocking layer (CBL) thickness	1
N_{CBL}/cm^{-3}	CBL doping concentration	1×10^{18}
H/μm	GaN drift layer thickness	10
H_1/μm	top (bottom) part thickness of n(p)-pillar in non-SJ HFET	1∼10
N_1/cm^{-3}	top (bottom) part doping concentration of n(p)-pillar in non-SJ HFET or doping concentration of n- and p-pillars in un-SJ HFET	$0.5\times10^{16}\sim2\times10^{16}$
H_2	bottom (top) part thickness of n(p)-pillar in non-SJ HFET	H minus H_1
N_{step}/cm^{-3}	doping concentration increment in non-SJ HFET	$1\times10^{16}\sim2.5\times10^{16}$
N_2	bottom (top) part doping concentration of n(p)-pillar in non-SJ HFET	N_1+N_{step}
W_N (W_P)/μm	n-pillar (p-pillar) width ($W_N=W_P$)	5

3. On-state and off-state analyses

Figure 2 shows the on-state *I*–*V* characteristics for non-SJ HFET and un-SJ HFET. In Fig. 2(a), both devices exhibit the same threshold voltage of about 0.6 V. The drain current of the proposed non-SJ HFET is greater than that of un-SJ HFET when the gate voltage is beyond the threshold voltage, indicating a smaller on-state resistance in non-SJ HFET. In addition, comparing with un-SJ HFET, the obvious improvement of the slope of the *I*–*V* curve in the linear region could be seen from Fig. 2(b) in non-SJ HFET at the same bias. This results in a smaller $R_{on}A$ of 1.784 mΩ·cm^2 in non-SJ HFET than that of 2.597 mΩ·cm^2 in un-SJ HFET, thus leading to more than 31% decrease in $R_{on}A$. From the off-state *I*–*V* performance in Fig. 3, both devices exhibit the same breakdown voltage of 1800 V. Therefore, the significant reduction in $R_{on}A$ could be realized by means of nonuniform doping superjunctions at no expense of *BV*, which demonstrates a better trade-off between *BV* and $R_{on}A$ in non-SJ HFET.

A physical insight into the improvement in non-SJ HFET could be achieved according to on-state current density distributions as well as off-state equipotential lines and electric field distributions. At on-state for both devices in Fig. 4(a), only the n-pillar can conduct current because the n$^+$ substrate/p-pillar junctions and the n-pillar/p-pillar junctions are under the reversed bias condition. The current path width along the horizontal direction in n-pillar will be shrunk by the depletion effect to a certain degree. As shown, a similar current path width could be observed in the top part N_{N1} of the n-pillar in non-SJ HFET and the corresponding position in un-SJ HFET. Comparing with un-SJ HFET, the current path in the bottom part N_{N2} of the n-pillar in the non-SJ HFET is obviously widened, which is attributed to the higher doping concentration in the bottom part N_{N2} of the n-pillar. From Fig. 4(b), a greater current density could be seen in the n-pillar of the non-SJ HFET. Therefore, both the wider current path and the greater current density in non-SJ HFET are beneficial to the current conduction and then the reduction in $R_{on}A$.

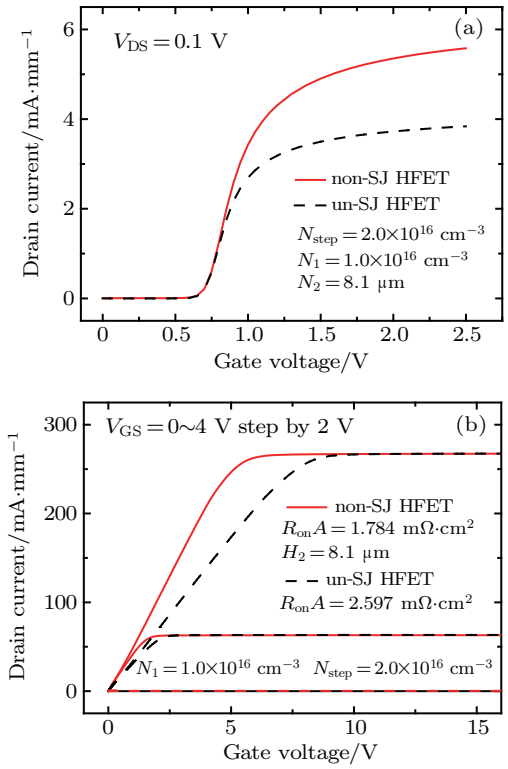


Fig. 2. (color online) On-state *I*–*V* characteristics for two devices, showing (a) transfer characteristics, (b) output characteristics.

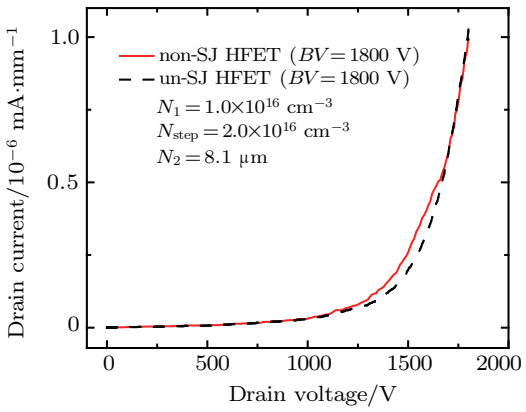


Fig. 3. (color online) Off-state *I*–*V* characteristics corresponding to the devices in Fig. 2.

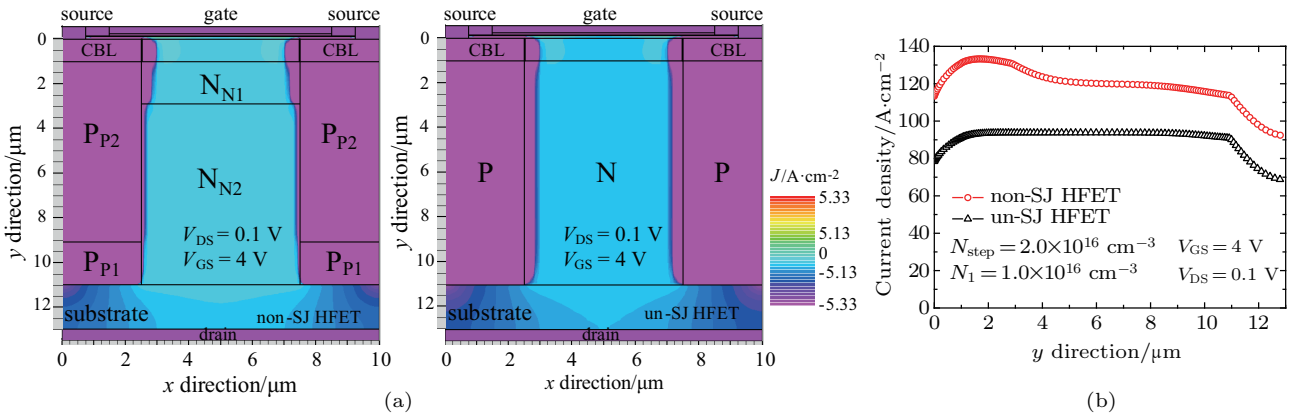


Fig. 4. (color online) On-state current density distributions corresponding to the devices in Fig. 2, showing (a) two-dimensional distributions, and (b) distributions along line B1B2 as shown in Fig. 1.

The breakdown performances in non-SJ HFET and un-SJ HFET are illustrated in Fig. 5. Comparing with un-SJ HFET, in non-SJ HFET the equipotential lines densities near the middle of n- and p-pillars increase slightly while those near the bottom of n- and p-pillars decrease slightly in Fig. 5(a). This implies that the electric field strength near the middle is enhanced while that near the bottom is degraded in n- and p-pillars, which could be demonstrated by the vertical electric field distributions along the line A1A2 in Fig. 5(b). As shown, the area beneath the contour of each electric field distribution can be used to estimate the *BV* of each device approximately.[4] Equal areas could be observed in both devices, and thus indicating the same *BV*.

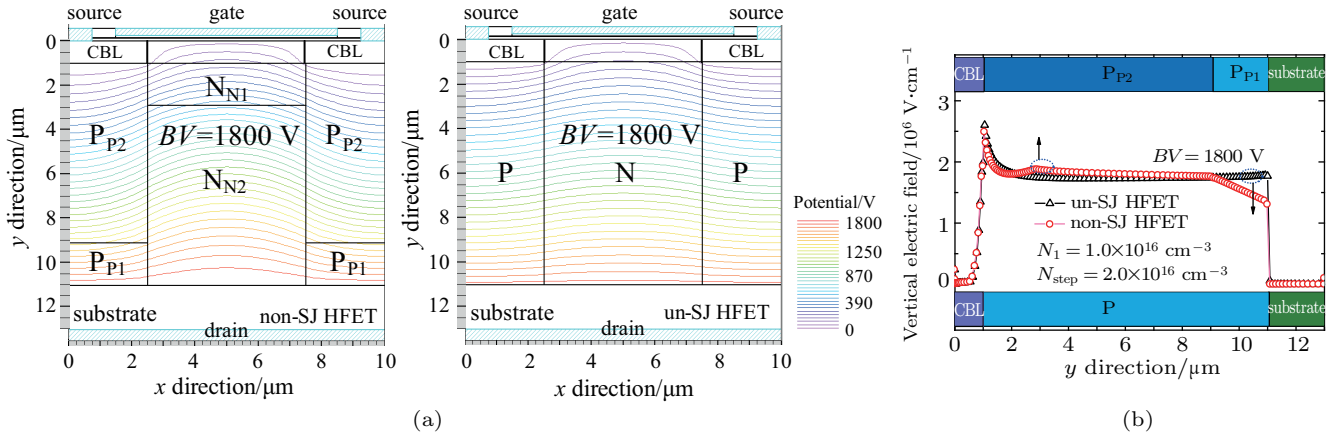


Fig. 5. (color online) Off-state performances in two devices at breakdown voltage corresponding to Fig. 3. (a) Equipotential lines distribution, and (b) electric field distribution along line A1A2 as shown in Fig. 1.

4. Optimization and design for minimized $R_{on}A$ without deterioration in *BV*

Figure 6 shows the plots of breakdown voltage and specific on-resistance versus thickness H_2 at different values of N_1 for a given N_{step} in non-SJ HFET. It is noted that the structure of non-SJ HFET will be changed into that of un-SJ HFET when $H_2 = 0$ μm. As shown, for each concentration N_1, the $R_{on}A$ decreases continuously with H_2 increasing. This results from the increase in the average doping concentration of n-pillar. Besides, there exists a peak *BV* at $H_2 = 4$ μm for each N_1. For a given H_2, both *BV* and $R_{on}A$ decrease with N_1 increasing. The variations of *BV* and $R_{on}A$ with N_1 in un-SJ HFET are also consistent with the reported results in Ref. [11]. The optimized H_2 is determined by minimizing $R_{on}A$ on the basis of the same *BV* as that of un-SJ HFET, which means the maximum reduction in $R_{on}A$ at no expense of *BV*. It could be found that the optimized H_2 appears to be nearly 8 μm and will decrease slightly with the increase in N_1. If H_2 is beyond the optimal value, the *BV* of non-SJ HFET will be lower than that of un-SJ HFET for a given N_1. When N_1 varies from 0.5×10^{16} cm^{-3} to 2×10^{16} cm^{-3}, the optimized $R_{on}A$ will drop from 2.292 mΩ· cm^2 to 1.498 mΩ·cm^2, indicating a corresponding reduction from 48.8% to 15.5% compared with the scenario of un-SJ HFET. Figure 7 shows the vertical electric field distributions along the line A1A2 in non-SJ HFETs with different values of H_2. As shown in the figure, the electric field strength around the middle of pillar is raised obviously for $H_2 = 4$ μm, leading to the largest area beneath the contour of electric field distribution and thus the greatest *BV*. In the same way, the lowest *BV* appears in the case of $H_2 = 9$ μm because of the smallest area. These features of electric field distributions could provide an appropriate explanation for the variations of *BV* with H_2 in Fig. 6.

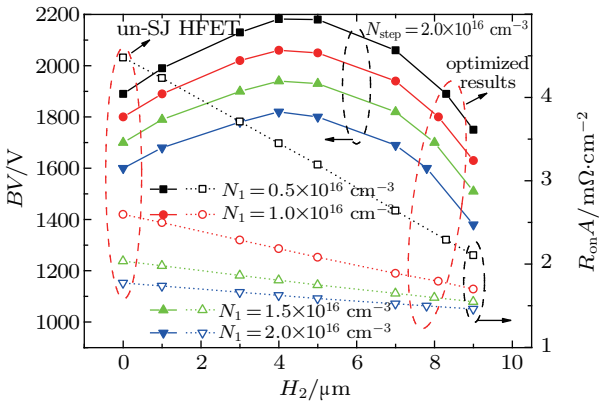


Fig. 6. (color online) Plots of breakdown voltage and specific on-resistance versus H_2 at different values of N_1 for a given N_{step} in non-SJ HFET.

Figure 8 shows the plots of breakdown voltage and specific on-resistance versus H_2 at different values of N_{step} for a given N_1. For each N_{step}, the $R_{on}A$ will drop as H_2 increases. Further, it could be seen clearly that the decrement in $R_{on}A$ will be raised with N_{step} increasing for a given H_2. The variation of *BV* with H_2 for each N_{step} is similar to that in Fig. 6 and the peak *BV* appears at $H_2 = 4$ μm. On the basis of the same *BV* as that of un-SJ HFET, the optimized H_2 for each N_{step} is obtained to minimize $R_{on}A$. As shown, this optimized H_2 will increase a little with N_{step} increasing.

According to the minimum $R_{on}A$ corresponding to each optimized H_2 in the non-SJ HFET, the reduction of $R_{on}A$ in the non-SJ HFET compared with the un-SJ HFET, could be calculated and depicted in Fig. 9. The reductions in $R_{on}A$ for other optimized results at different values of N_1 achieved by the method in Fig. 8 are also shown in Fig. 9, and the values of BV in non-SJ HFETs with different values of N_1 are also equal to those in un-SJ HFETs with the same N_1. For each N_1, the reduction in $R_{on}A$ could be improved by increasing N_{step}. The remarkable reduction in $R_{on}A$ could be obtained in the case of lower N_1 and higher N_{step}. The maximum reduction of 51.1% in $R_{on}A$ could be realized for $N_1 = 0.5 \times 10^{16}$ cm^{-3} and $N_{step} = 2.5 \times 10^{16}$ cm^{-3}. Even when $N_1 = 2 \times 10^{16}$ cm^{-3} and $N_{step} = 1 \times 10^{16}$ cm^{-3}, the reduction of 9.8% could still be achieved. These improvements further demonstrate the superiority and effectiveness of non-SJ HFET in minimizing $R_{on}A$ at no expense of BV.

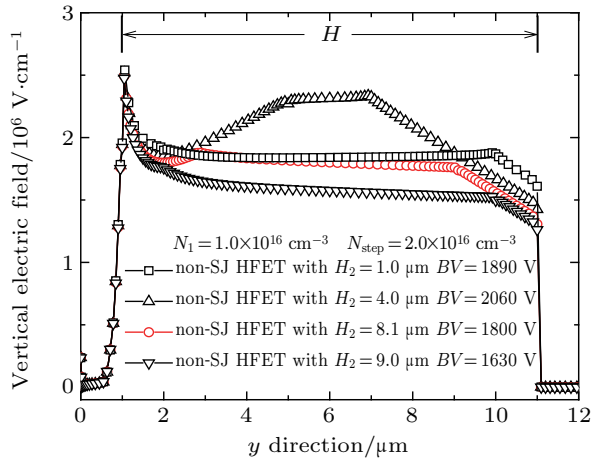


Fig. 7. (color online) Vertical electric field distributions along the line A1A2 in corresponding non-SJ HFETs with different values of H_2 in Fig. 6.

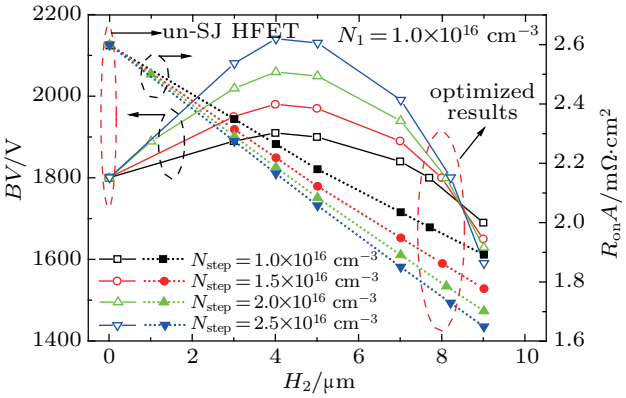


Fig. 8. (color online) Plots of breakdown voltage and specific on-resistance versus H_2 at different values of N_{step} for a given N_1 in non-SJ HFET.

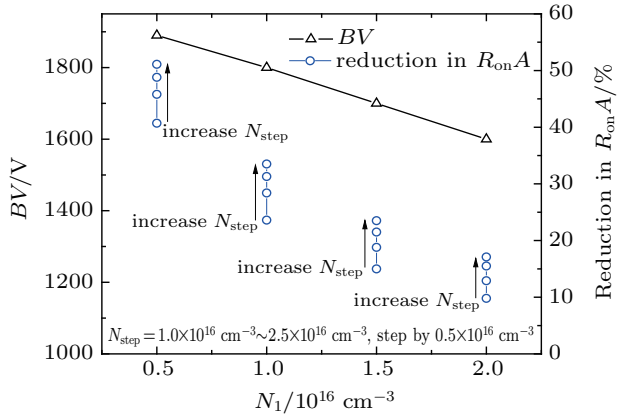


Fig. 9. (color online) BV and reductions in $R_{on}A$ for optimized results at different values of N_1 and N_{step}.

5. Fabrication process

Nowadays, thick *in situ* doping GaN layer growth technologies,[22,23] GaN-based selective area growth technologies (SAG),[14,24] and GaN etching technologies have become more and more mature.[25,26] The reported highest GaN pillar height by SAG and the deepest etching trench by plasma etching technology have been more than 10 μm,[27,28] which could pave the way for fabricating the non-SJ HFET. Therefore, the proposed non-SJ HFET may be realized by SAG technology, during which the n-pillar and p-pillar will be grown alternately. This fabrication proposal has also been considered as a possible way to realize the conventional un-SJ HFET in Ref. [11].

As an example, the following gives a feasible process approach of the proposed non-SJ HFET based on the methods mentioned in Refs. [14] and [24], as illustrated in Fig. 10. Firstly, a p-type GaN layer with N_1 doping and H_1 thickness is epitaxially grown by metal–organic chemical vapor deposition (MOCVD) on a bulk GaN substrate. Then trench-1 with W_N width and H_1 thickness is formed by the Cl-based inductively coupled plasma (ICP) etching process. The rest of the p-type GaN layer is masked and an n-type GaN layer with N_2 doping and H_1 thickness is regrown by SAG to fill trench-1. Secondly, a p-type GaN layer with N_2 doping and (H_2 minus H_1) thickness is epitaxially grown by MOCVD followed by the trench-2 etching and the SAG regrowth of n-type GaN layer with N_2 doping in the trench. Thirdly, a p-type GaN layer with N_2 doping and H_1 thickness and the 1-μm CBL layer are epitaxially grown by MOCVD followed by the trench-3 etching and the SAG regrowth of n-type GaN layer with N_1 doping in the trench. The final main procedures comprise the regrowth of the GaN channel and $Al_{0.15}Ga_{0.85}N$, the growth and etching of P^+-GaN cap, the source/drain/gate contact metal and passivation layer deposition and the isolation deep etching of GaN, after which the completed device is obtained and shown in Fig. 10(j).

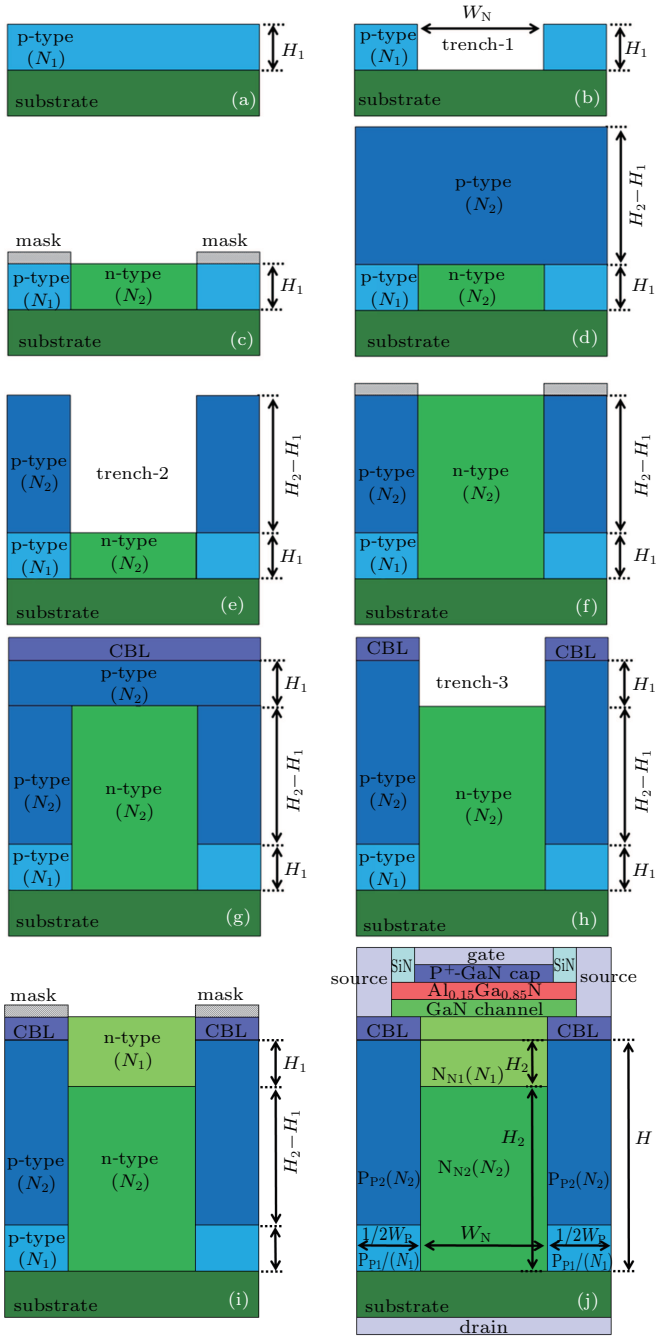


Fig. 10. (color online) A feasible process approach of the proposed non-SJ HFET, showing (a) (N_1 doping and H_1 thickness) p-type GaN layer growth, (b) trench-1 etching, (c) n-type GaN layer regrowth in trench-1, (d) (N_2 doping and H_2–H_1 thickness) p-type GaN layer growth, (e) trench-2 etching, (f) n-type GaN layer regrowth in trench-2, (g) (N_2 doping and H_1 thickness) p-type GaN layer and CBL growth, (h) trench-3 etching, (i) n-type GaN layer regrowth in trench-3, and (j) completed device.

6. Conclusions

In this paper, a novel non-SJ HFET based on the nonuniform doping superjunctions (non-SJs) is presented by two-dimensional simulations, with emphasis on the minimized $R_{on}A$ at no expense of BV. Systematical studies and analyses of the device on- and off-state performance, device physical mechanisms as well as device optimization designs are conducted. The simulation results exhibit that the remarkable reduction in $R_{on}A$ with the same BV as that of un-SJ HFET, could be realized by modulating the doping concentration and thickness of the light and heavy doping parts in non-SJ. These results demonstrate the potential and advantage of non-SJ HFET in high power electronic applications.

References

[1] Wang L, Hu W D, Chen X S, Lu W 2010 *Acta Phys. Sin.* **59** 5730 (in Chinese)

[2] Mao W, Yang C, Hao Y, Zhang J C, Liu H X, Ma X H, Wang C, Zhang J F, Yang L A, Xu S R, Bi Z W, Zhou Z, Yang L, Wang H 2011 *Acta Phys. Sin.* **60** 017205 (in Chinese)

[3] Huang H, Liang Y C, Samudra G S, Chang T F and Huang C F 2014 *IEEE Trans. Power Electron.* **29** 2164

[4] Mao W, Fan J S, Du M, Zhang J F, Zheng X F, Wang C, Ma X H, Zhang J C, Hao Y 2016 *Chin. Phys. B* **25** 127305

[5] Li S P, Zhang Z L, Fu K, Yu G H, Cai Y, Zhang B S 2017 *Acta Phys. Sin.* **66** 197301 (in Chinese)

[6] Zhang L, Lin Z Y, Luo J, Wang S L, Zhang J C, Hao Y, Dai Y, Chen D Z, Guo L X 2017 *Acta Phys. Sin.* **66** 247302 (in Chinese)

[7] Chowdhury S, Wong M H, Swenson B L and Mishra U K 2012 *IEEE Electron Dev. Lett.* **33** 41

[8] Mal S, Agarwal A, Ahmadi E, Bhat K M, Ji D, Laurent M A, Keller S and Chowdhury S 2017 *IEEE Electron Dev. Lett.* **38** 933

[9] Saito W, Kuraguchi M, Takada Y, Tsuda K, Omura I and Ogura T 2005 *IEEE Trans. Electron Dev.* **52** 106

[10] Shrestha N M, Wang Y Y, Li Y M and Chang E Y 2015 *Vacuum* **118** 59

[11] Li Z D and Chow T P 2013 *IEEE Trans. Electron Dev.* **60** 3230

[12] Du J F, Liu D, Zhao Z Q, Bai Z Y, Li L, Mo J H and Yu Q 2015 *Superlattices Microstruct.* **83** 251

[13] Du J F, Liu D, Bai Z Y, Liu Y, Yu Q 2015 *Superlattices Microstruct.* **85** 690

[14] Nie H, Diduck Q, Alvarez B, Edwards A P, Kayes B M, Zhang M, Ye G, Prunty T, Bour D and Kizilyalli I C 2014 *IEEE Electron Dev. Lett.* **35** 939

[15] Chowdhury S and Mishra U K 2013 *IEEE Trans. Electron Dev.* **60** 3060

[16] Yeluri R, Lu J, Hurni C A, Browne D A, Chowdhury S, Keller S, Speck J S and Mishra U K 2015 *Appl. Phys. Lett.* **106** 183502

[17] Ambacher O, Smart J, Shealy J R, Weimann N G, Chu K, Murphy M, Schaff W J, Eastman L F, Dimitrov R, Wittmer L, Stutzmann M, Rieger W and Hilsenbeck J 1999 *J. Appl. Phys.* **85** 3222

[18] Mnatsakanov T T, Levinshtein M E, Pomortseva L I, Yurkov S N, Simin G S and Khan M A 2003 *Solid-State Electron.* **47** 111

[19] Oğuzman I H, Bellotti E, Brennan K F, Kolník J, Rongping W, and Ruden P P 1997 *J. Appl. Phys.* **81** 7827

[20] Vurgaftman I, Meyer J R and Ram-Mohan L R 2001 *J. Appl. Phys.* **89** 5815

[21] Piprek J 2003 *Semiconductor optoelectronic devices: Introduction to physics and simulation* (California: Elsevier Science)

[22] Usikov A, Kovalenkov O, Soukhoveev V, Ivantsov V, Syrkin A, Dmitriev V, Nikiforov A Y, Sundaresan S G, Jeliazkov S J and Davydov A V 2008 *Phys. Stat. Sol.* **5** 1829

[23] Paskova T, Hanser D A and Evans K R 2010 *Proc. IEEE* **98** 1324

[24] Tourret J, Gourmala O, Andre Y, Trassoudaine A, Gil E, Castelluci D and Cadoret R 2009 *J. Cryst. Growth* **311** 1460

[25] Cho H K, Khan F A, Adesida I, Fang Z Q and Look D C 2008 *J. Phys. D: Appl. Phys.* **41** 155314

[26] Liu Z C, Pan J L, Asano A, Ishikawa K, Takeda K, Kondo H, Oda O, Sekine M and Hori M 2017 *Jpn. J. Appl. Phys.* **56** 026502

[27] Hartmann J, Steib F, Zhou H, Ledig J, Nicolai L, Fündling S, Schimpke T, Avramescu A, Varghese T, Trampert A, Straßburg M, Lugauer H J, Wehmann H H and Waag A 2017 *J. Cryst. Growth* **476** 90

[28] Harrison S E, Voss L F, Torres A M, Frye C D, Shao Q H and Nikolic R J 2017 *J. Vac. Sci. Technol. A* **35** 061303